






Article

Assessing the Impact of Clearing and Grazing on Fuel Management in a Mediterranean Oak Forest through Unmanned Aerial Vehicle Multispectral Data

Luís Pádua ^{1,2,3,*} , João P. Castro ^{4,5} , José Castro ⁶ , Joaquim J. Sousa ^{3,7}  and Marina Castro ^{4,5} 

- ¹ Centre for the Research and Technology of Agro-Environmental and Biological Sciences (CITAB), University of Trás-os-Montes e Alto Douro, 5000-801 Vila Real, Portugal
- ² Institute for Innovation, Capacity Building and Sustainability of Agri-Food Production, University of Trás-os-Montes e Alto Douro, 5000-801 Vila Real, Portugal
- ³ Engineering Department, School of Science and Technology, University of Trás-os-Montes e Alto Douro, 5000-801 Vila Real, Portugal; jjsousa@utad.pt
- ⁴ Centro de Investigação de Montanha (CIMO), Instituto Politécnico de Bragança, 5300-253 Bragança, Portugal; jpmc@ipb.pt (J.P.C.); marina.castro@ipb.pt (M.C.)
- ⁵ Laboratório Associado para a Sustentabilidade e Tecnologia em Regiões de Montanha (SusTEC), Instituto Politécnico de Bragança, 5300-253 Bragança, Portugal
- ⁶ Departamento de Ambiente e Recursos Naturais, Escola Superior Agrária, Instituto Politécnico de Bragança, 5300-253 Bragança, Portugal; mzeicast@ipb.pt
- ⁷ Centre for Robotics in Industry and Intelligent Systems (CRIIS), Institute for Systems and Computer Engineering, Technology and Science (INESC-TEC), 4200-465 Porto, Portugal
- * Correspondence: luispadua@utad.pt

Abstract: Climate change has intensified the need for robust fire prevention strategies. Sustainable forest fuel management is crucial in mitigating the occurrence and rapid spread of forest fires. This study assessed the impact of vegetation clearing and/or grazing over a three-year period in the herbaceous and shrub parts of a Mediterranean oak forest. Using high-resolution multispectral data from an unmanned aerial vehicle (UAV), four flight surveys were conducted from 2019 (pre- and post-clearing) to 2021. These data were used to evaluate different scenarios: combined vegetation clearing and grazing, the individual application of each method, and a control scenario that was neither cleared nor purposely grazed. The UAV data allowed for the detailed monitoring of vegetation dynamics, enabling the classification into arboreal, shrubs, herbaceous, and soil categories. Grazing pressure was estimated through GPS collars on the sheep flock. Additionally, a good correlation ($r = 0.91$) was observed between UAV-derived vegetation volume estimates and field measurements. These practices proved to be efficient in fuel management, with cleared and grazed areas showing a lower vegetation regrowth, followed by areas only subjected to vegetation clearing. On the other hand, areas not subjected to any of these treatments presented rapid vegetation growth.

Keywords: remote sensing; unmanned aerial vehicles; grazing monitoring; forest management; normalized difference vegetation index; land use; land cover change; vegetation dynamics; sustainable fuel management; wildfire prevention



Citation: Pádua, L.; Castro, J.P.; Castro, J.; Sousa, J.J.; Castro, M. Assessing the Impact of Clearing and Grazing on Fuel Management in a Mediterranean Oak Forest through Unmanned Aerial Vehicle Multispectral Data. *Drones* **2024**, *8*, 364. <https://doi.org/10.3390/drones8080364>

Academic Editor: Eben N. Broadbent

Received: 10 June 2024

Revised: 24 July 2024

Accepted: 29 July 2024

Published: 31 July 2024



Copyright: © 2024 by the authors. Licensee MDPI, Basel, Switzerland. This article is an open access article distributed under the terms and conditions of the Creative Commons Attribution (CC BY) license (<https://creativecommons.org/licenses/by/4.0/>).

1. Introduction

Southern Europe is greatly impacted by wildfires, primarily due to climate conditions and the type of vegetation cover [1]. This region experiences an average of 47,000 fires annually, destroying 400,000 hectares of natural and forested land between 1980 and 2019 [2]. This scenario worsened in 2022, with more than 660,000 hectares burned between 1 January and 12 August, as reported by the European Forest Fire Information System (EFFIS) [3]. This is 56% higher than the previous record set in 2017 (420,913 hectares) for the same period. Wildfire incidence has dramatically increased over the last decades, with the

average burned area quadrupling since the 1960s [1]. This cause is mainly due to landscape homogenization, fuel load accumulation, and rural depopulation after the Second World War [4]. Climate change has made wildfires more dangerous, increasing in magnitude and severity [5]. Without effective action on land and fuel load management, reversing the trend of increasing wildfires will be challenging. Fuel load is considered the most important factor in fire management [6], as it supplies the energy for ignition and spread, modulating fire intensity and severity [7,8]. Additionally, years of fire suppression practices may play a role, particularly in vegetation biomes, with some of the highest fire frequency rates [9].

Reducing fuel load at the stand level and creating landscape discontinuities are seen as effective strategies for preventing wildfires [10]. Pastoral systems are very common along the Mediterranean region and provide an opportunity to manage the fuel load and reduce ecosystem fire risk [11–13]. Recently, the Open2preserve project [14] has been experimenting with strategies such as combining grazing with prescribed burning and/or mechanical treatments like thinning and shrub clearing to reduce fuel accumulation. Such actions add value by providing several positive effects on rural livelihoods and the environment, contributing to sustainable rural development [13,15–18]. Continuous monitoring of pastures is critical for monitoring their quality and grazing pressure. However, there is a need for techniques that efficiently and systematically monitor pasture cover changes for effective grazing management [19].

Remote sensing platforms can monitor areas, evaluate the characteristics of active fires, and characterize post-fire ecological effects and vegetation dynamics [20]. Unmanned aerial vehicles (UAVs) have increased the spatial resolution of remotely sensed data [21] for land use and land cover classification (LULC) [22]. UAVs are flexible tools for remote sensing data acquisition due to their ability to acquire data at different spatial, temporal, and radiometric resolutions [23]. UAVs are used in several vegetation studies to assess vegetation geometric and biophysical features, nutrient content and deficiencies, water stress, weeds, and disease detection [24]. Above-ground biomass (AGB) is an important indicator of ecosystem carbon storage [25], and UAV-based data can be used to assess AGB and above-ground volume (AGV) through spectral indices and/or structural metrics [26]. Studies have shown the effectiveness of UAV-based data for biomass estimation in shrubland communities [26–28]. UAV-based data is also used to map AGB in grassland and forage communities through the computation of vegetation indices from multispectral [29–32] or RGB data [33–35]. Topographical features or heights can also be included [29,30,34]. Recent studies have assessed forage quality mapping through UAV imaging spectroscopy [36,37]. Data from this platform can also be used for pasture and grazing monitoring, including the spatial and temporal changes in the pasture, grazing rotation needs [38,39], pasture intake estimation during grazing [40], and pasture biomass estimation [41]. UAV-based data can estimate tree positions and heights in agrosilvopastoral systems [42]. In the case of fire disturbances, UAV-based data can estimate fire severity by comparing pre- and post-fire differences [43], as well as the effects of fire and grazing on trees, shrubs, and herbaceous vegetation in savannah ecosystems [44]. Other studies explored AGB estimation from terrestrial LIDAR data [27,45] and airborne LIDAR and imagery data [46]. Photogrammetric dense point clouds from close-range imagery [47] have also been used for this purpose. These sensors can be used to obtain very high-resolution data, but those are often more expensive and/or laborious [48–50].

Studies on the temporal changes of pasture lands using UAV-based or remote sensing data are limited in number. This article presents a study aimed at evaluating the structure of the understory vegetation of an open Mediterranean forest in northeastern Portugal in plots subjected to four different treatments (control, clearing without grazing, clearing and grazing, grazing without clearing). To achieve this goal, the plots were monitored for three years, and high-resolution multispectral images were acquired over four different periods. This sets the study apart from others that only evaluate one season in controlled experimental plots [31,33,38]. In addition, the study compares two methods of assessing vegetation structure: the line intercept method (traditional field measurement [51]) and the

UAV-based method. The traditional methods for determining understory vegetation (herbaceous or shrub vegetation) involve collecting data along transects in the field by trained technicians. Using UAV-based photogrammetric products can provide a quicker and less labor-intensive alternative to obtain such data [52], which can be suitable for small to medium-sized areas [49] or for mapping specific locations with multiple photographs [30].

2. Materials and Methods

2.1. Study Area

The study was conducted in an open Mediterranean forest in the “Romeu” Natura 2000 Site of Community Importance in northeast Portugal (SIC PT CON0043). The experimental area covers approximately 4.5 hectares ($41^{\circ}32'25''$ N, $7^{\circ}02'16''$ W), with an altitude ranging between 480 m and 537 m (mean of 514 m). The location of this area within Portugal's mainland is presented in Figure 1a. The dominant vegetation consists of an open mixed sclerophyllous forest with *Quercus faginea*, *Q. rotundifolia*, and *Q. suber* and a shrub layer with *Cistus ladanifer*, *Cytisus multiflorus*, and *Lavandula stoechas*. The presence of various species in this semi-natural forest leads to natural heterogeneity and soil fertility gradients, resulting in differences in floristic composition and in the shrub size due to the steep slope of the study area. The soils are classified as District Leptosols [53], according to the FAO/UNESCO Soil Map of the World [54]. These soils, commonly found in the Trás-os-Montes e Alto Douro region (northeastern Portugal), are derived from schist and are characterized by low fertility and degradation due to long-term cultivation. The heterogeneous landscape presents challenges for the flock's decision-making in terms of foraging and refuge. The study area was chosen due to the multiple strata present, reducing the influence of the flock's preferences.

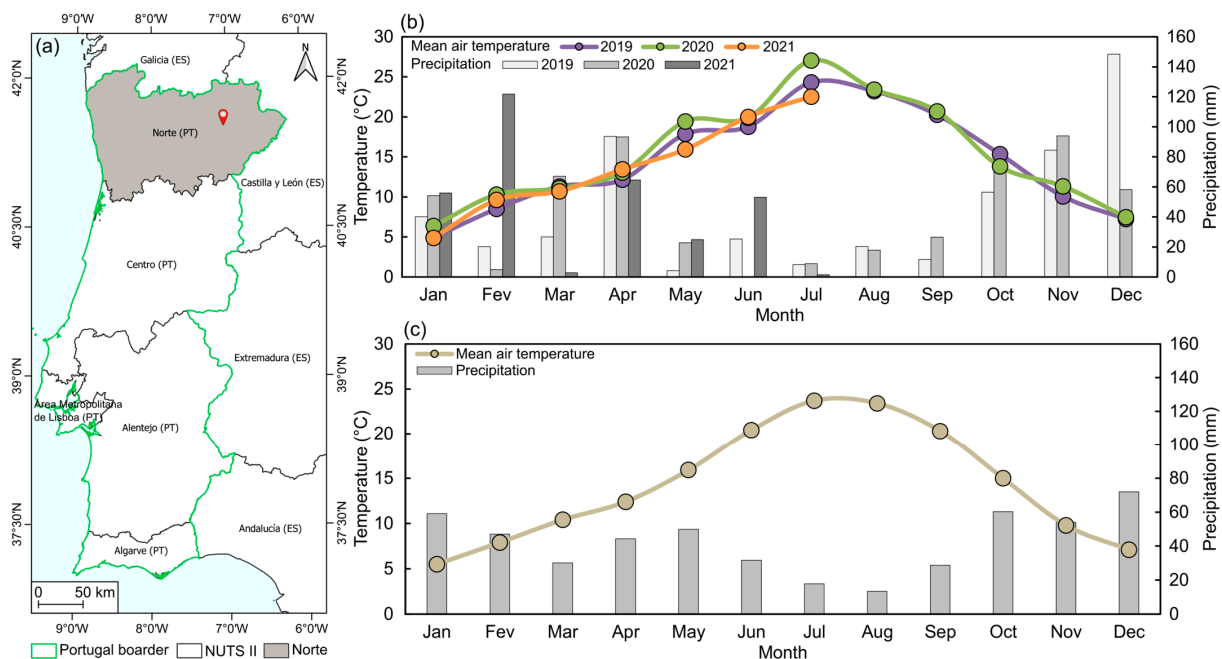


Figure 1. Location of the study site within Portugal's mainland and its NUTS (Nomenclature of Territorial Units for Statistics) II regions (a). Monthly mean temperature and accumulated precipitation in the study area between January 2019 and July 2021 (b,c) the climatological normal of Mirandela (data from the Portuguese Institute for Sea and Atmosphere, IPMA, Lisbon, Portugal).

The study area is located in the Mediterranean region, with a Meso-Mediterranean and a dry ombrotype. Figure 1b shows the monthly precipitation and temperature data from the monitored period (2019 to July 2021), obtained from the Europe-wide E-OBS temperature and precipitation gridded dataset v25.0e [55]. During the monitored period,

a wetter pattern occurred, along with a significantly higher average temperature in 2020. These inter-annual fluctuations are typical in the Mediterranean climate, as evidenced by changes in the standardized 30-year series (Figure 1c). The average annual temperature is 14.3 °C, and the total annual precipitation is 508.6 mm, based on the data from 1971–2000 of the town of Mirandela (Figure 1c).

2.2. Experiment Description

In May 2019, a vegetation clearing procedure was conducted to remove understory vegetation. The clearing was conducted through mechanical means using a 1.5 m wide chain shredder, and trees were not subjected to any management. The area was fenced after mechanical clearing (Figure 2a), and grazing began in December 2019 with a flock of approximately 150 native sheep (*Churra Galega Bragançana*), which were monitored using three GPS collars. Within the fenced area, a plot of 380 m² was kept from grazing and served as the “cleared and not grazed” treatment (being enclosed as shown in Figure 2c), while the rest of the fenced area was subjected to grazing. This included 1110 m² “not cleared”, the “not cleared and grazed” treatment, and two “cleared and grazed” plots of 1360 m² and 1970 m². Two additional plots outside the fenced area were used as a control treatment, which was neither cleared nor purposely grazed. The sizes of these plots were 457 m² and 1106 m². The treatment plots (polygons in Figure 2a) were defined according to the transects, which were permanently marked on the ground and used to determine herbaceous and shrub volume using the intercepting line method [56] (example in Figure 2b). Twelve transects were established on the ground, each 20 m long, with four in each treatment inside the fenced area. The location of these transects can be seen in Figure 2a.

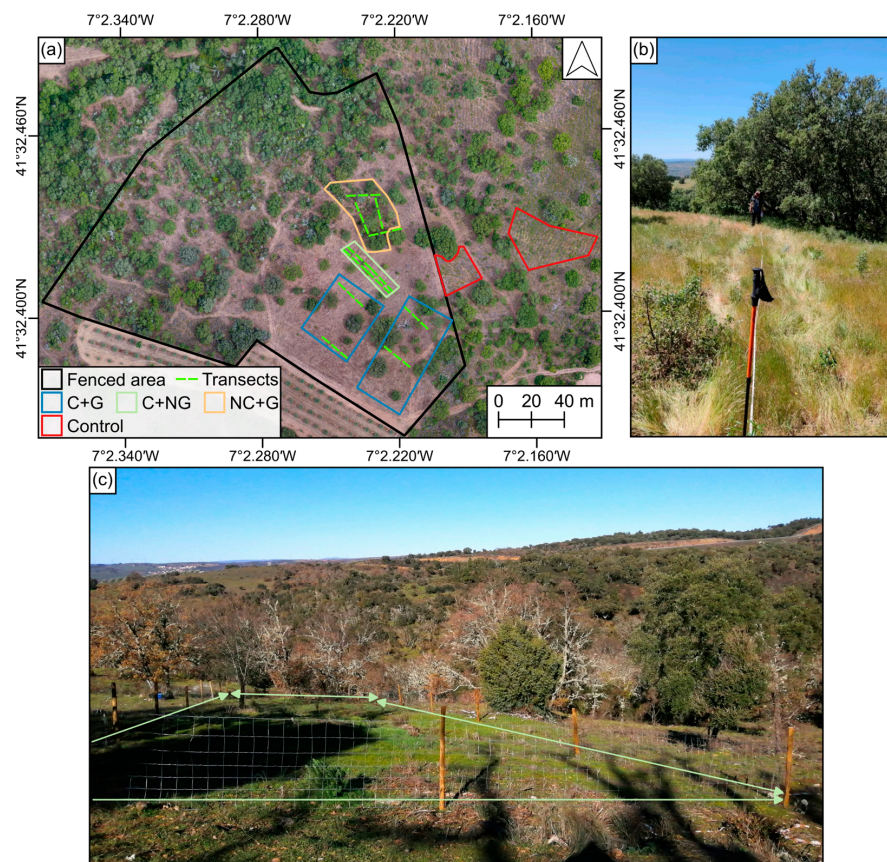


Figure 2. Study area overview: (a) spatial arrangement of the treatment plots, transects and fenced area after vegetation clearing operations; (b) vegetation volume determination using the intercepting line method (as of May 2021); and (c) cleared and not grazed plot, fenced after vegetation clearing. C: Cleared; G: Grazed; NC: Not cleared; NG: Not grazed.

The arrangement presented in Figure 2a allows the study of the effect of different treatments on vegetation structures with fire prevention in mind through fuel management. The plot size differences reflect the study being conducted on a private property representative of the analyzed territory. Larger plots were placed for study in areas with the greatest possible amount of grass for the flock's nutritional satisfaction. Smaller plots were placed in areas of less interest for grazing, just enough to evaluate the treatments "cleared and not grazed" and "grazed and not cleared".

2.3. Remote Sensing Data Acquisition

To monitor the vegetation dynamics over the duration of the study, UAV-based high-resolution aerial imagery was acquired in the visible and near-infrared (NIR) regions of the electromagnetic spectrum. For that purpose, a Phantom 4 (DJI, Shenzhen, China) was used. This multirotor UAV was equipped with a 12.4 MP RGB sensor coupled to a three-axis electronic gimbal. The Sequoia sensor (Parrot SA, Paris, France), installed in the UAV through a custom mount, was used for multispectral data acquisition. This sensor is composed of a camera array allowing the acquisition of green (530–570 nm), red (640–680 nm), red edge (730–740 nm), and NIR (770–810 nm) single-band images, with a 1.2 MP resolution. A sensor positioned at the top of the UAV was responsible for acquiring irradiance data during the flight. Before the flight mission, a target was used for reflectance calibration purposes. Both measurements were later used for radiometric calibration of the multispectral data.

Four flight campaigns were conducted between 2019 and 2021, with two flights per campaign. The flight parameters are presented in Table 1. The first flight in each campaign was for RGB imagery acquisition, while the second flight mission was for multispectral data acquisition. Ground control points (GCPs) were placed throughout the study area, and their XYZ coordinates were obtained using a Global Navigation Satellite System (GNSS) receiver in real-time kinematic (RTK) mode for centimeter precision.

Table 1. Flight parameters for the RGB and multispectral data acquisition, including flight height from the take-off position, flight pattern, image overlap and the approximate spatial resolution.

Sensor	Flight Height (m)	Flight Pattern	Image Overlap (Longitudinal/Lateral)	Approx. Spatial Resolution (m)
RGB	60	Double grid	80%/70%	0.04
Multispectral	90	Single grid		0.11

Flight missions were conducted before vegetation clearing on 25 February 2019 and after clearing on 3 July 2019, 6 July 2020, and 1 July 2021. This approach enabled the assessment of vegetation evolution over time, starting from the vegetation dynamics zero point (mechanical clearing).

2.4. Data Processing

2.4.1. Photogrammetric Processing

The aerial imagery from each flight was processed using Pix4DMapper Pro (Pix4D SA, Lausanne, Switzerland). It ensured a complete pipeline for correction, alignment, and radiometric calibration, producing dense point clouds and orthorectified raster products.

Initially, the acquired images were loaded, and a sparse point cloud was generated based on key points within the images. After this, GCPs were marked in the images to ensure a proper alignment between data acquired from both sensors and between different survey periods, enabling direct comparisons between different campaigns. The sparse point cloud was then reoptimized, and with the data properly aligned, a high-density point cloud was generated and classified. This point cloud was interpolated to produce an orthophoto mosaic (for RGB imagery), a digital surface model (DSM), a digital terrain model (DTM), and a canopy height model (CHM), which was generated by subtracting

DTM altitude values from the DSM. The CHM is calculated in QGIS software. In projects using multispectral data, radiometric calibration was performed before generating the raster outputs. Orthorectified reflectance maps were produced for each band, and the normalized difference vegetation index (NDVI) [57] was calculated using the NIR and red bands. The NIR, green, and red bands were also used to create false color compositions.

2.4.2. Vegetation Classification

The results obtained from the UAV-based photogrammetric processing have various applications. The orthophoto mosaics provide a visual assessment of the surveyed area, while the NDVI maps allow the analysis of the vegetative vigor, and the CHM provides the height of the vegetation above the ground. Based on the photointerpretation of the orthophoto mosaics and the values of CHM and NDVI, different types of vegetation cover can be classified according to Table 2. The classification categorizes each pixel as (1) soil or dried-up vegetation, (2) herbaceous vegetation, (3) shrubs, or (4) trees. The differentiation between herbaceous and shrub vegetation is based on the height value and the 0.3 m threshold, which was determined through the knowledge of the study area (as seen in Figure 2b) and the photointerpretation of the UAV data. The grazable shrub stratum was between 0.3 m and 1.5 m. NDVI values for live vegetation were always greater than 0.35. These threshold values could be adjusted based on the study area characteristics.

Table 2. Pixel classification into one of the four classes and the criteria used for the canopy height model (CHM) and normalized difference vegetation index (NDVI) raster products.

Class ID	Class	Classification Criteria		
		CHM Value(s) (m)		NDVI Value
1	Soil/Others	≤ 0.05	or	< 0.35
2	Herbaceous	≤ 0.30	and	≥ 0.35
3	Shrubs	> 0.30 and ≤ 1.50	and	≥ 0.35
4	Trees	> 1.50	and	≥ 0.35

Additionally, the classification maps calculated as described in Table 2 were used to generate new CHM and NDVI products that replaced pixels belonging to arboreal vegetation with no-data values. These new NDVIs were used to calculate the difference NDVI (dNDVI) by subtracting the pre-clearing NDVI from a specific post-clearing season NDVI, as expressed in (1).

$$dNDVI_i = NDVI_i - NDVI_{pre-clearing} \quad (1)$$

The dNDVI values allow for comparison between any sampling date and the pre-clearing state. Negative values indicate that non-arboreal elements are less vigorous than their original state, while positive values suggest that non-arboreal elements are developing to or above their pre-clearing condition.

2.5. Data Analysis

The UAV-based multi-temporal data were used to assess the dynamic of the vegetation over time for the different treatments (presented in Figure 2a) by comparing the evolution of each treatment with the initial stage and with the other treatments. Furthermore, the impact of grazing was evaluated by comparing cleared and grazed areas with cleared-only treatments over the various survey periods after vegetation clearing. Other comparisons, such as cleared and grazed and grazed-only treatments, were also analyzed. For this purpose, in each plot, the cover percentage of each class was evaluated over time. In this analysis, the vegetation volume and mean NDVI values for each plot were also considered. Evaluations were carried out using data discarding tree canopy. The UAV-based volume was estimated for each treatment in each sampling period and was obtained from the CHMs and land cover maps to exclude arboreal vegetation. The height of each CHM

pixel was multiplied by its pixel area to calculate canopy volume (CV), as described in Mao et al. [26]. This volumetric variable represents the space between the outer surface of the vegetation canopy and the ground, incorporating the combination of plant parts and void space. To standardize results and facilitate direct comparison, the CV of each treatment plot was converted to cubic meters per hectare. A preliminary assessment of volume estimation was performed by correlating the estimated UAV-based CV with the field-measured volume. The Pearson correlation coefficient (r) was calculated to determine the correlation between measured and estimated volume.

The three GPS collars installed to monitor the sheep flock provided data that could be used to generate grazing pressure maps, which serve as a way to monitor grazing activity over time in the study area. The monitoring took place from December 2019 to June 2021, using data from the five months prior to the UAV surveys in 2020 and 2021. For a more accurate grazing pressure analysis, only the locations of the collar with the highest number of records for each grazing day were used. To effectively distinguish grazing pressure across the study area, heatmaps were produced using a 55 m radius (the longest distance to the nearest neighboring location) and an output pixel size of 1.5 m (half the average distance between the closest records) by following the methods described in Hengl [58].

3. Results

3.1. Analysis of the UAV-Based Data Products

The first flight campaign coincided with the start of the Open2preserve project (February 2019), which reflects the reality of the site just before the vegetation clearing. The subsequent flight campaigns took place in July 2019, 2020, and 2021, coinciding with the summer season. By comparing the orthophoto mosaics from February 2019 and July 2019 (Figure 3), one can see the absence of the herbaceous and shrub vegetation that resulted mainly from late winter clearing and grazing of the spring shoots. The presence of leaves on deciduous tree species is also noticeable, particularly in the false color composition (Figure 3b). In the orthophoto mosaics from 2020 and 2021, the differences in vegetation between cleared and non-cleared and grazed and non-grazed treatments, as well as the regeneration of the vegetative cover and growth of tree crowns, can be visualized. In areas subjected to heavy grazing, a reduction in available feed is expected, which will be evaluated by the proposed methodology.

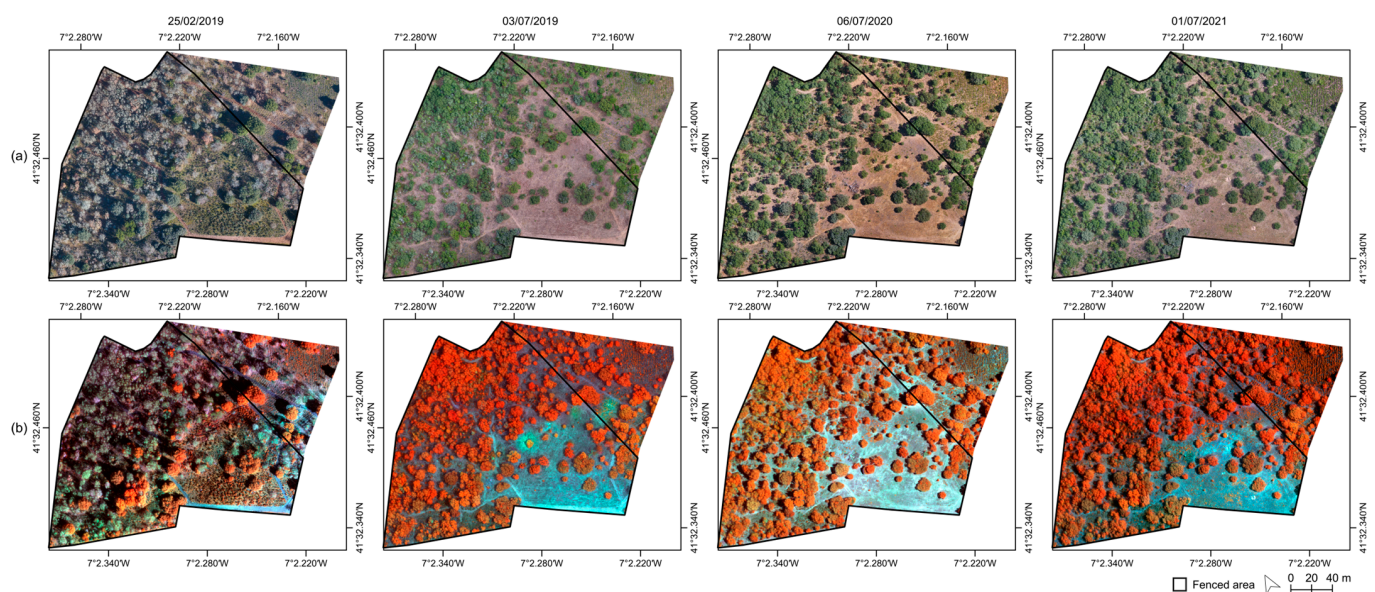


Figure 3. Overview of the studied site at the different periods surveyed from orthophotos of true (a) and false color compositions (b). Near-infrared, green, and red bands were used to create the false-color compositions.

The NDVI raster products generated from the multispectral data (Figure 4a) enabled the analysis of the vegetative vigor along the flight campaigns. When analyzing the NDVI raster statistics within the fenced area (Table 3), the maximum value always exceeded 0.9, and a lower mean value was observed in the pre-clearing flight (0.5). The mean NDVI value increased in the first post-clearing flight campaign (July 2019), decreased in 2020 (from 0.55 to 0.53), and increased to the highest value in 2021 (0.6). The minimum values decreased from the first to the second flight campaign, increased in 2020, and decreased in 2021. Higher NDVI standard deviation values were recorded in the post-clearing flight campaigns. Figure 4b shows the height distribution of the surveyed area: it has a predominance of taller vegetation (i.e., trees) in the northwestern and northern regions, while the central and southern parts have a higher concentration of low vegetation or bare soil. In the fenced area, the maximum value was approximately 15 m in the pre-clearing flight campaign (February 2019) and increased to almost 18 m in the remaining flight campaigns. The mean height value rose from 2.1 m to 2.6 m from the pre-clearing to the post-clearing flight campaigns, and the standard deviation followed a similar trend (from 2.6 m to 3.0 m). In 2020 and 2021, the mean CHM values were 2.4 m and 2.6 m, respectively.

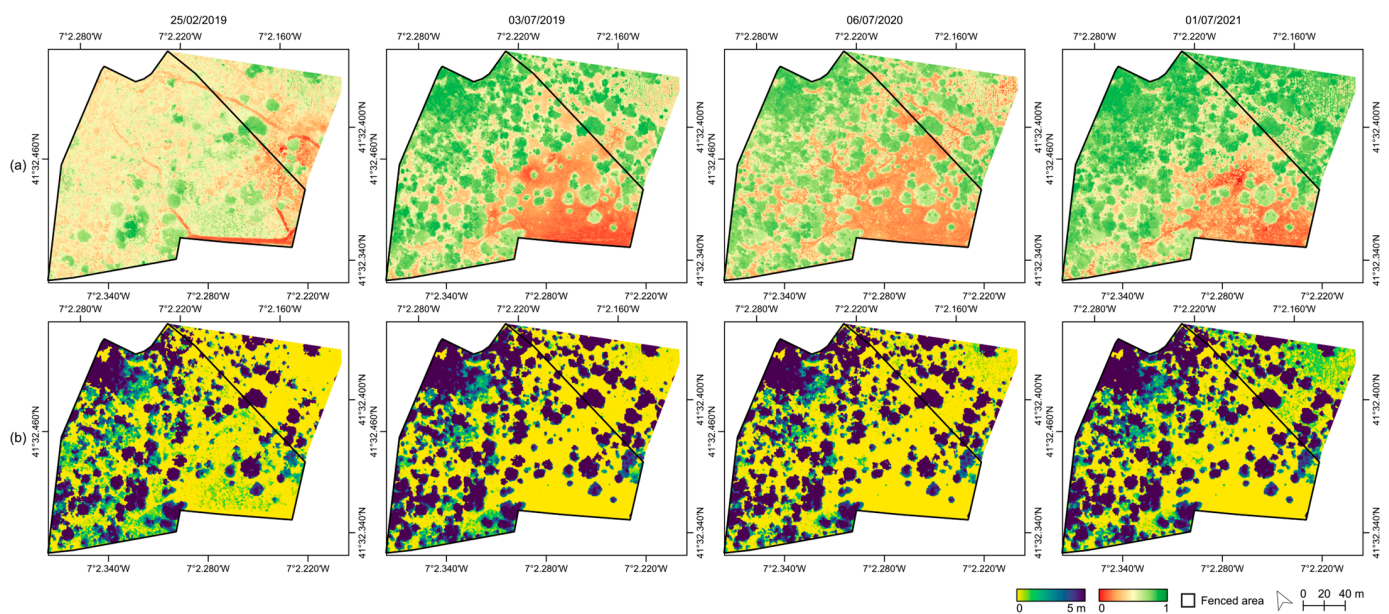


Figure 4. Normalized difference vegetation index (a) computed from the multispectral data in each surveyed period and the canopy height models (b) computed from the photogrammetric processing of the RGB imagery.

Table 3. Basic statistics (maximum, mean, minimum, and standard deviation) of the normalized difference vegetation index in each flight campaign. Values considering only the fenced area.

Date	Max.	Mean	Min.	SD
25 February 2019	0.95	0.50	−0.24	0.14
3 July 2019	0.92	0.55	−0.32	0.25
6 July 2020	0.91	0.53	−0.15	0.22
1 July 2021	0.93	0.60	−0.19	0.23

3.2. Multi-Temporal Vegetation Monitoring

3.2.1. General Characterization of the Study Area

The vegetation classification method described in Section 2.4.2. was applied to the raster products from each flight campaign to characterize the four defined land cover classes present in the study area (spatial distribution in Figure 5). Before clearing, the data showed a predominance of herbaceous vegetation along with arboreal vegetation.

After vegetation clearing, herbaceous vegetation decreased, and the majority of the area was classified as soil, which decreased over time and changed to herbaceous and shrub vegetation in some areas.

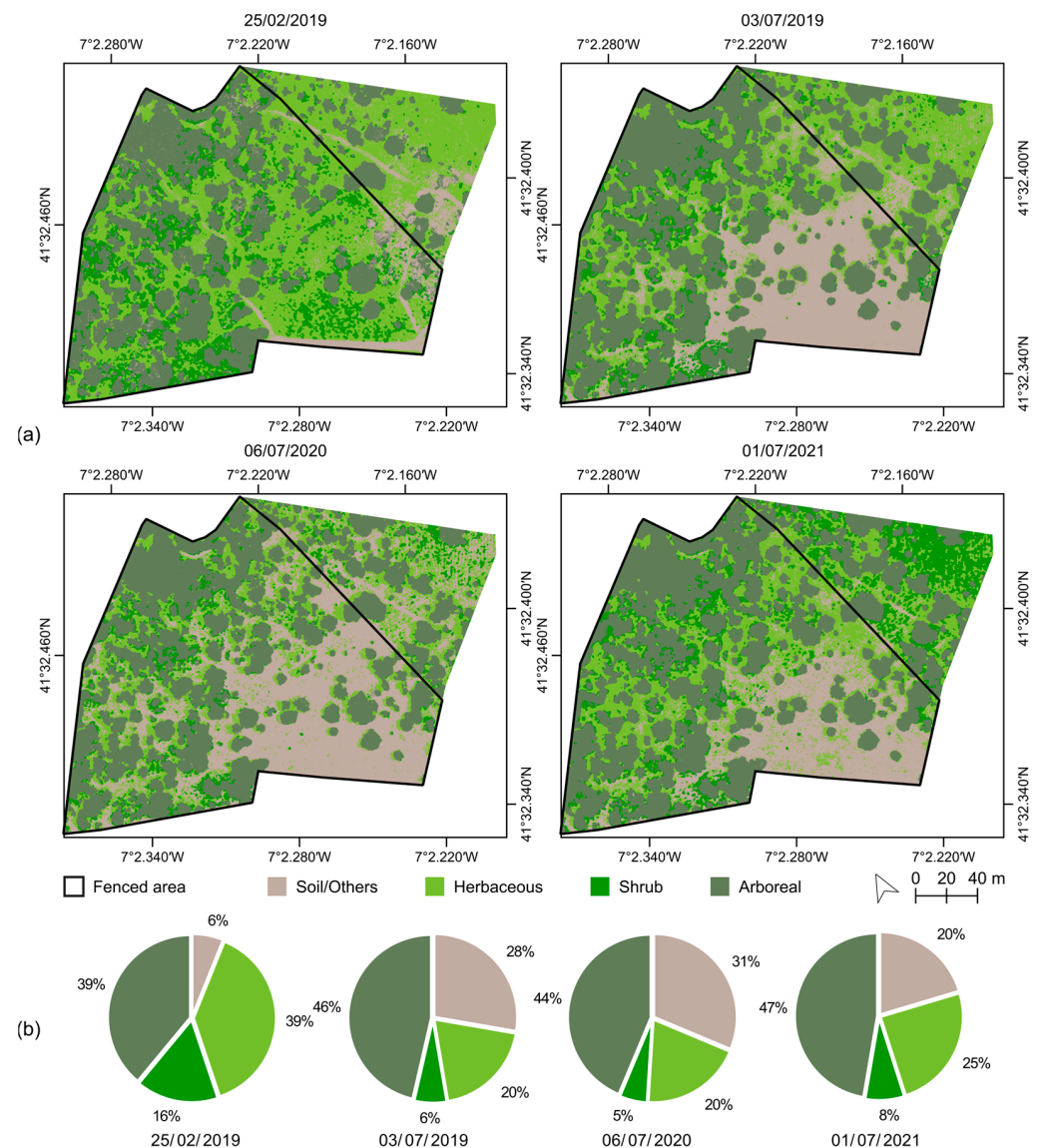


Figure 5. Land cover distribution over the surveyed periods (a) and the overall percentage of each class within the fenced area (b).

To closely examine the land cover changes over time in the study area, the percentage of each land cover class was calculated within the fenced area (Figure 5). The land cover distribution from the first flight campaign showed only 6% (0.2 ha) occupied by bare soil or dried-up vegetation, followed by shrub vegetation (16%, 0.5 ha) and arboreal and herbaceous vegetation, which represented 78% of the total land cover (each with 39%, 1.3 ha). After the clearing operations, a 22% increase in soil cover was found, occupying 28% of the fenced area (0.9 ha), and arboreal vegetation increased by 7% (46% of the area covered, corresponding to 1.5 ha). In contrast, both herbaceous and shrub vegetation decreased by 29% (−0.9 ha), representing 26% of the fenced area. In the two subsequent flight campaigns (2020 and 2021), no major changes were found. Soil increased to 31% (1.1 ha) in 2020 and decreased to 20% (0.7 ha) in 2021. Arboreal vegetation covered an area of 44% and 47% (1.5 and 1.6 ha) in 2020 and 2021, respectively. Shrub vegetation decreased to 5% (0.2 ha) in 2020, while herbaceous vegetation maintained a 20% land occupation.

However, in 2021, both herbaceous and shrub vegetation covered 33% (1.1 ha), representing an increase of 3% in the shrub occupation and 5% of the herbaceous vegetation.

3.2.2. Treatment Plots

An overview of the different treatment plots in each surveyed season is shown in Figure 6. The percentage of cover type in each plot was also analyzed, and a single result was calculated for the control and cleared and grazed treatments despite being composed of two polygons.

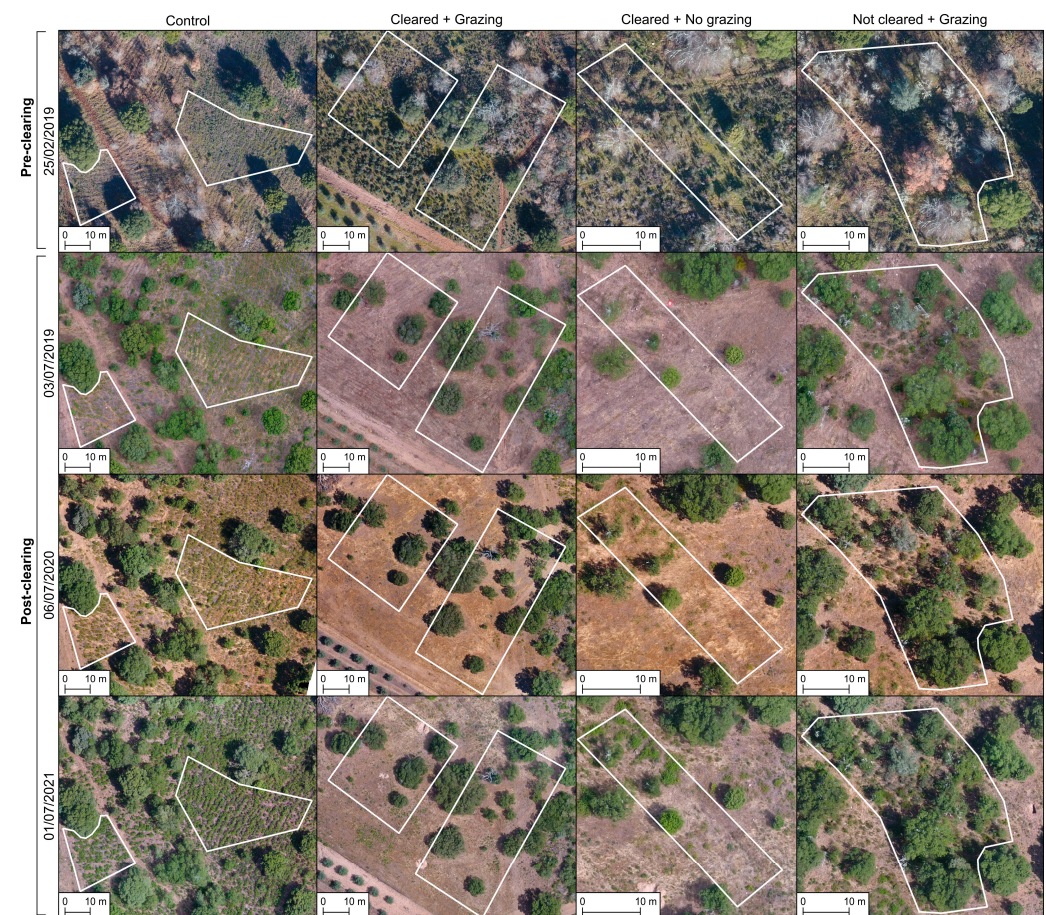


Figure 6. Overview of the different analyzed treatment plots (white polygons) in the different surveyed periods (February 2019 and July 2019, 2020, and 2021).

The multi-temporal analysis of the non-arboreal cover types revealed each different vegetative trend for treatment over time (Figure 7). The control treatments, which were cleared and nor purposely grazed and were located outside the fenced area, demonstrated an increase in both herbaceous and shrub cover from February 2019 to July 2021. In February 2019, 92% of the cover was herbaceous vegetation, while 1% was shrub vegetation. In July 2019, both soil and shrubs increased to 24% and 3%, respectively; this trend was also found in July 2020 and 2021. By July 2021, shrub cover had increased from 64%, while herbaceous vegetation and soil represented 31% and 5%, respectively. This means that the control treatment's potential fuel increased to 95% (excluding soil). The treatment that was not cleared but subjected to grazing showed a decline in shrub vegetation cover, resulting in an increase in soil cover from 1% in February 2019 to 20% in July 2020. Herbaceous vegetation and shrub communities decreased to 67% and 12%, respectively. However, by July 2021, the soil cover had decreased to 2%, while herbaceous and shrub vegetation had increased to 99%, similar to the cover percentage in February 2019. Treatment plots that were subjected to vegetation clearing showed an increase in soil cover in the first post-clearing flight campaign

(July 2019). The treatment plots that were grazed showed a lower vegetative cover than the not-grazed plots in 2020 (18% vs. 27%) and 2021 (24% vs. 48%).

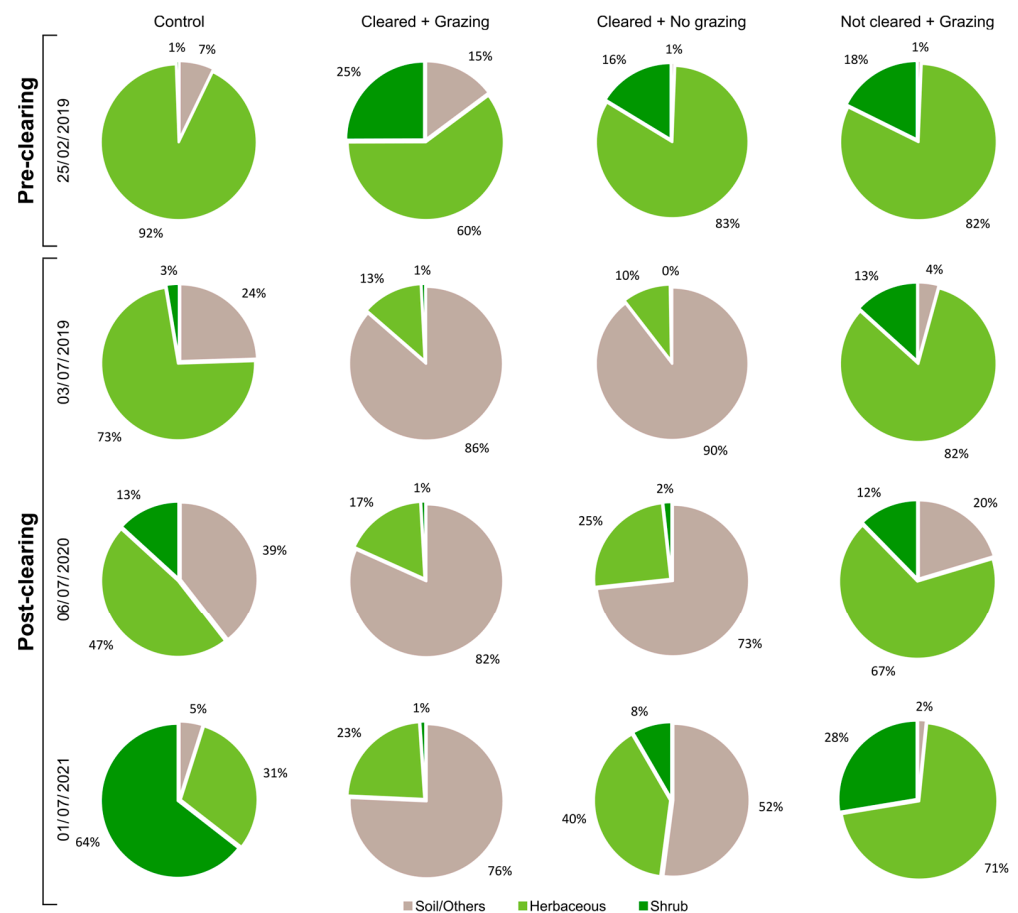


Figure 7. Overall percentage of land cover over the surveyed periods, excluding arboreal vegetation.

The NDVI maps were computed to measure vegetation density, with arboreal vegetation excluded. The mean NDVI values for each treatment were calculated for different seasons and are shown in Figure 8a. The pre-clearing results (February 2019) indicate that the plot that was not cleared and not grazed had the highest mean NDVI value (0.55), followed by the not-cleared and grazed plot (0.54), the cleared and grazed plot (0.47), and the control plot with the lowest mean NDVI value (0.46). Vegetation clearing was noticeable for both treatments that were subjected to this procedure. An abrupt decrease in the mean NDVI values was found from the pre- to post-clearing. In contrast, the non-cleared treatments showed only a small decrease (−0.02). In July 2019, the highest average NDVI value was found in the treatment that was not cleared but grazed, followed by the control treatment, and both cleared treatments had the lowest average values. From July 2019 to 2021, the mean NDVI values in the treatments that were not cleared showed a slight decrease, while the opposite was observed in the cleared areas. However, the treatment that was cleared and not grazed had a higher mean NDVI value than the treatment that was cleared and grazed. From July 2020 to 2021, the mean NDVI value increased in all treatment plots except for the cleared and grazed plots. In the last surveyed data, the control treatment had the highest mean NDVI value (0.66), followed by the treatment that was not cleared and grazed (0.64) and the treatment that was cleared and not grazed (0.40), and the lowest mean value was observed in the cleared and grazed treatment (0.27).

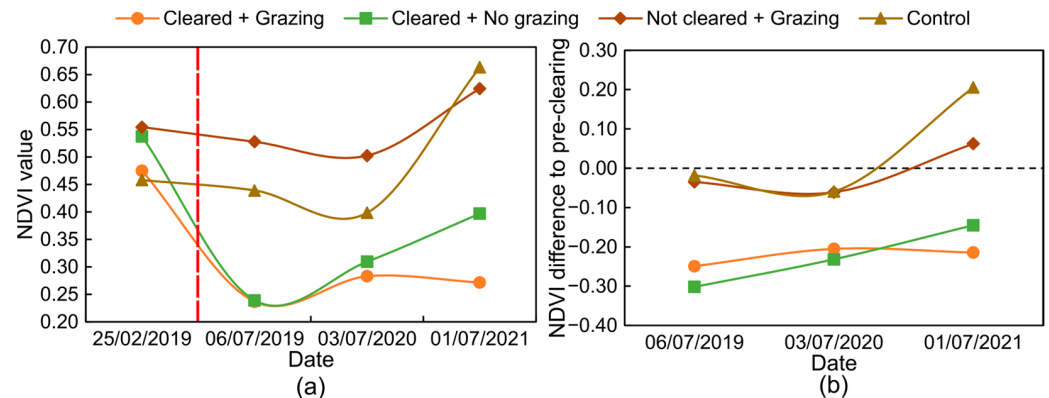


Figure 8. Mean NDVI value per treatment plot over time (a) and the NDVI difference post-clearing compared with pre-clearing (b). The clearing time is marked with the red line.

The results from the dNDVI analysis (Figure 8b) demonstrated the trend of growth or decline across the survey periods. Initially, all values were negative during the first two seasons after clearing. However, a positive dNDVI was observed in the control and in the not-cleared and grazed treatments, indicating vegetation growth beyond pre-clearing levels.

The CV of each treatment in each sampling period is shown in Figure 9a, excluding arboreal vegetation. Before vegetation clearing, the highest CV was observed for the cleared and grazed treatment (around $2600 \text{ m}^3 \text{ ha}^{-1}$), followed by the cleared and not-grazed treatment (around $1380 \text{ m}^3 \text{ ha}^{-1}$). The control treatment had the lowest CV ($187 \text{ m}^3 \text{ ha}^{-1}$), while the cleared and not-grazed treatment had an estimated CV of $1109 \text{ m}^3 \text{ ha}^{-1}$. After the first post-clearing flight campaign (July 2019), all treatments had less than $1000 \text{ m}^3 \text{ ha}^{-1}$, with a decrease in all treatments within the fenced area, except for the control treatment, which increased by 170% (Figure 9b). In July 2020, CV increased in all treatments except for the cleared and grazed treatment (-32% to $481 \text{ m}^3 \text{ ha}^{-1}$). The control and the not-cleared and grazed treatments showed a CV increase of over 100% (126% and 198%, respectively). In July 2021, the control treatment had a 359% increase, while the cleared and grazed treatment decreased by 25%. The “cleared and not grazed” and “not cleared and grazed” treatments increased by 34% and 54%, respectively. At the end of the surveyed period, the control treatment had the highest estimated CV ($5228 \text{ m}^3 \text{ ha}^{-1}$), followed by the not-cleared and grazed treatment ($1260 \text{ m}^3 \text{ ha}^{-1}$) and the cleared and not-grazed treatment ($922 \text{ m}^3 \text{ ha}^{-1}$), with the lowest estimated CV in the cleared and grazed treatment ($361 \text{ m}^3 \text{ ha}^{-1}$).

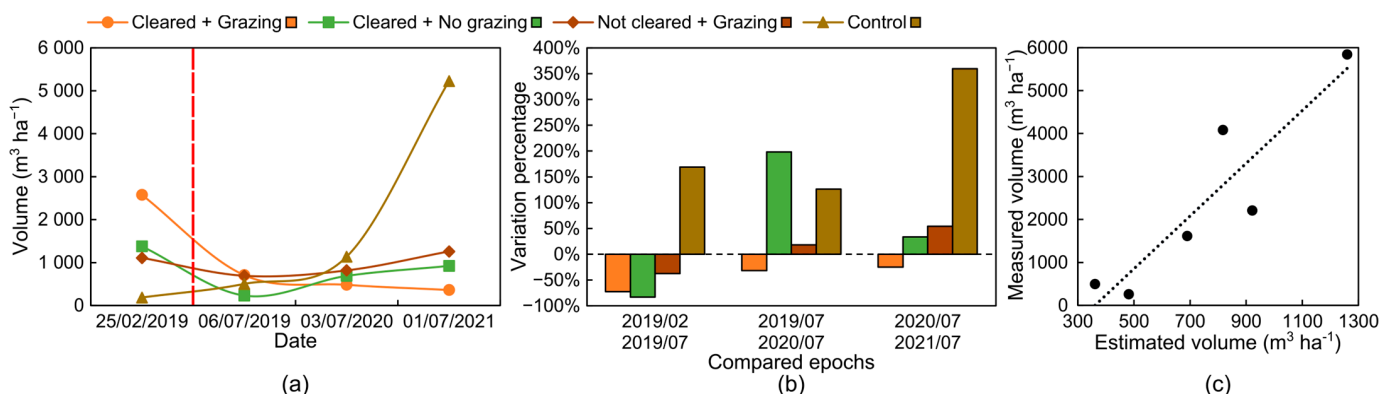


Figure 9. Volume for each treatment plot estimated for different periods (a), its variation percentage when compared to the previous flight campaign (b), and the comparison between field measurements and UAV-based data (c). The clearing time is marked with the red line.

The transects placed within the treatment plots (location in Figure 2) were used to assess the correlation the measured vegetation volume and estimated CV. This approach

was compared to the CV estimated from the UAV-based data (Figure 9c) by using the mean volume for each treatment from the data of 15 July 2020 and 25 May 2021. An r value of 0.91 was obtained, indicating a good relationship between the two variables. Despite the high correlation, the CV estimated from UAV-based data showed underestimation.

3.3. Grazing Pressure

The fenced area was grazed by a local flock of about 150 sheep (Section 2.2). The livestock husbandry system involved daily grazing circuits in the agropastoral landscape, comprising owned, rented, and borrowed land, including the study area and adjacent pastures. The duration of the grazing circuit varies throughout the year based on factors such as daylight, maximum daily temperature, and resource availability. The variation of grazing pressure on the study area from the winter to summer solstices, at 6-month intervals, was evaluated. From December 2019 to June 2020, the flock was in the study area for about 52 days (totaling 88 h) and from December 2020 to June 2021 for 89 days (totaling 132 h). Figure 10 shows the grazing pressure maps, each of which represents the density of GPS records obtained using three GPS collars in the previous five months before each flight campaign. The GPS records were collected every five minutes whenever the animal was moving, had communication via satellite, and had a battery.

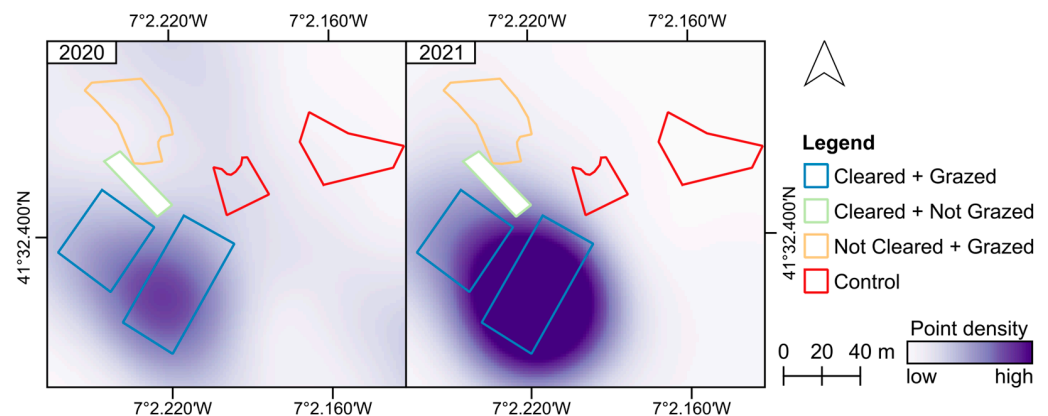


Figure 10. Grazing pressure density maps based on the point density of the GPS collars, with data computed from the five months prior to the flight campaigns in 2020 and 2021.

As shown in Figure 10, the highest grazing pressure was observed in the cleared and grazed plots in both periods, with a greater occurrence in the months prior to the 2021 flight campaign. Although the not-cleared and grazed plot also experienced an increase in grazing pressure, it still remains lower compared with the cleared areas.

4. Discussion

The vegetation-clearing procedure is evident in the computed NDVI maps (Figure 4), which show the differences between pre- and post-clearing periods due to both seasonal changes and a decrease in the mean NDVI and CHM values (Table 3 and Figure 4). Despite this, height estimates from UAV photogrammetric data have demonstrated a good agreement in various studies [41,59–61]. The winter season, when the deciduous trees have no leaves, provides a better understanding of their crown structure, as seen in the pre-clearing flight data (February 2019, Figure 3). However, the reliability of the CHM could be affected by height underestimations in leafless trees [44,62]. CHM maps were also used in other studies for multi-temporal monitoring of forage grasslands [34]. The decrease in the mean NDVI values between the first and second flight campaigns is primarily attributed to the vegetation-clearing operation. Changes between flight campaigns are also noticeable in the CHM; the presence of leaves on deciduous trees (mostly oaks) in the post-clearing flights (July 2019, 2020 and 2021) led to an increase in the mean height value. This allowed for the

observation of the vegetation-clearing operation between the first two campaigns, as well as vegetation growth in areas that were not cleared.

The vegetation cover type analysis (Figure 7) demonstrated the impact of clearing on shrub cover. The cleared plus grazing treatment showed almost no shrub cover, while the non-cleared treatments showed a higher percentage of shrubs. The reduction in shrub cover between July 2019 and July 2020 in the grazed areas demonstrated the effectiveness of grazing as a sustainable approach to vegetation control and fire risk reduction. Multi-temporal analysis of NDVI changes over analyzed periods (Figures 9 and 10) showed that treatments subjected to clearing had lower NDVI values compared with non-cleared treatments, with the control treatment having the highest mean NDVI values in the last flight campaign. Meanwhile, the cleared and grazed treatment showed the lowest values of NDVI and dNDVI. In other studies, dNDVI has been used as a tool for evaluating fire severity [43] and vegetation regeneration [63]. The use of other vegetation indices besides NDVI can also be considered [30]. Théau et al. [31] used similar approaches to this study to classify vegetation cover in grassland but did not consider the use of CHM, and instead of using NDVI, they used GNDVI [64]. The authors defined different intervals to classify the study area over time into bare soil, low, medium, and high vegetation through the analysis of e^{GNDVI} values. The use of CHM could have improved the classification results. In the future, to assess the effect of grazing on understory volume (pixel by pixel) (m^3/m^2), another approach could be to separate the tree component from the shrub and herbaceous component and then multiply the area of each pixel by vegetation height (CHM) and vegetation index (e.g., NDVI), which is directly proportional to vegetative vigor.

The relationship between NDVI and grazing pressure is shown in the grazing pressure maps (Figure 10), which demonstrate the impact of grazing on vegetation. The cleared and grazed treatment area experiences the highest grazing pressure and exhibits the lowest NDVI and CV. On the other hand, the not-cleared and grazed treatment presented lower grazing pressure, resulting in higher NDVI and CV values, second only to the control treatment. This study highlights the importance of using UAV data together in combination with GPS collars for precision grazing management. Cattle geolocation and geographical information system (GIS) analysis can also be used to study their seasonal patterns [65]. Other studies have explored the use of UAVs for monitoring cattle behavior response to the presence of UAVs [66] and for livestock monitoring through its detection, counting, and distribution [67–69].

The correlation between volume estimates (Figure 9c) demonstrates the accuracy of interpreting the different treatments. Treatments with lower/higher volumes are more likely to be ranked in the same order if the volume is measured in the field. When comparing it with other studies that addressed biomass and volume estimation, the obtained correlation value ($r = 0.91$) is good, but the estimated values have a high underestimation. Despite this drawback, the UAV approach makes it possible to monitor large areas in a short period of time compared with more reliable but labor-intensive terrestrial methods. Other studies, such as Lussem et al. [33], obtained a coefficient of determination (R^2) from 0.57 to 0.73 for dry biomass and 0.43 to 0.79 for fresh biomass. Insua et al. [38] obtained an $R^2 = 0.80$ for pasture biomass. Abdullah et al. [28], in shrub AGB estimation, obtained an R^2 of 0.815, 0.740, and 0.245 for crown area, shrub volume, and shrub height, respectively. Moreover, Batistoti et al. [41] obtained an $R^2 = 0.74$ for pasture biomass in a Brazilian savanna. Studies that reported high correlation values often rely on more complex methodologies that require more labor or use more expensive equipment. For instance, Zhang et al. [30] used a non-linear logarithmic regression model and obtained an R^2 of 0.89 for grassland AGB estimation based only on mean height; Mao et al. [26] found the most significant contribution in AGV estimation through a regression model that incorporated CV and textural and spectral parameters obtaining an $R^2 = 0.928$; Zhao et al. [27] obtained an $R^2 = 0.83$ using multispectral imagery and an $R^2 = 0.86$ by combining multispectral and UAV LIDAR data for individual estimation for AGB in shrubs. Passalacqua et al. [47] obtained R^2 values between 0.90 and 0.96 for AGB estimation of grasslands using 3D point clouds acquired at

1 m above vegetation. The occasional differences in field- and UAV-based CV are due to the fact that transects under the canopy provide additional information that is not visible from the air. This problem may be solved with sensors that can penetrate the vegetation, such as LIDAR. Seasonal fluctuations between years may also contribute to differences in values. Other features, such as textural features or the sum of contrast values, could be explored, as those were among the most important AGB predictors in Zhao et al. [27], followed by volumetric, geometric, and spectral features.

The techniques applied in this study have the potential for wider application, with small adjustments, such as monitoring vegetation regeneration and fuel density in areas with a high risk of forest fire. This can be achieved through satellite-based data, although UAV-based data may be more accurate for biomass estimation [32]. UAV data can also be used for land cover classification and to improve the quality of satellite data by removing mixed pixels [70]. Increasing the frequency of monitoring throughout the year could provide insights into the short- and medium-term effects of grazing in pastures, as demonstrated by Alvarez-Hess et al. [40]. UAVs are also useful for monitoring grassland recovery during seasonal droughts [71]. Machine learning and more vegetation indices can improve land cover classification [72]. For example, Adar et al. [70] used machine learning to classify land cover in areas subject to intensive grazing and non-grazing, while Lu and He [73] used high-resolution UAV data to classify grassland species along the season, and Trenčanová et al. [74] used deep learning and UAV data to classify shrub cover.

Several limitations should be considered for improvement in future studies, such as the issue of discrimination between dried-up vegetation and bare soil, as the surveyed periods and the resolution of the UAV data have made it difficult to discriminate between dried-up vegetation and bare soil. To tackle this problem, aerial surveys should be conducted more frequently to identify the best soil moisture stage for the monitored area, probably during springtime. The location of the field data should be examined since transects below the tree canopy prevent a proper data validation of UAV-based results. Thus, those should be placed in open areas visible from the sky (without being covered by tree crowns), as well as using sampling points of at least 50×50 cm, enabling the acquisition of a larger number of samples in each treatment and the performance of regression analysis on vegetative volume. The grazing activities should be carried out equally for all treatments that are subjected to it by scheduling rotational grazing to ensure that all treatments have the equivalent grazing pressure. Moreover, if it is intended to study the effects of the different treatments in other situations (fertility gradients and spatial heterogeneity), there is a need to stratify the area beforehand and repeat the treatments in different situations.

5. Conclusions

This study provided insights into the effects of grazing, combined or not with mechanical clearing, on vegetation dynamics and demonstrated the usefulness of UAV-based methods in monitoring these effects. The UAV flight campaigns enabled the extraction of several variables from a single flight campaign. The use of multispectral and RGB data allowed us to calculate different variables, such as vegetation volume, vigor level, and land cover type. As expected, the most effective treatment for controlling understory scrub in open Mediterranean oak woodlands, thus reducing fire risk, is a combination of mechanical clearing and grazing. Grazing activities alone also demonstrated its effectiveness, as vegetation was managed, and the presence of shrub vegetation did not increase at the same rate as in the control treatment. The understory volume estimated from the UAV-based data showed a good correlation with the line-intercept method, confirming the feasibility of using UAV data to evaluate the effects of combined treatments (grazing and/or mechanical cleaning). This approach enables more extensive and timely monitoring of fuel loads and, consequently, fire risk. However, the relationship between vegetation moisture and the optimal timing for UAV flight surveys requires further investigation, as the herbaceous layer in aerial data can be confused with the bare soil class as it dries out.

Author Contributions: Conceptualization, J.P.C., J.C. and M.C.; data curation, L.P., J.P.C. and J.C.; formal analysis, L.P., J.C. and M.C.; funding acquisition, J.P.C., J.C. and M.C.; investigation, L.P., J.P.C., J.C. and M.C.; methodology, L.P., J.P.C., J.C., J.J.S. and M.C.; project administration, M.C.; resources, J.P.C., J.C., J.J.S. and M.C.; software, L.P.; supervision, J.P.C., J.J.S. and M.C.; validation, L.P., J.C., J.J.S. and M.C.; visualization, L.P. and J.C.; writing—original draft, L.P., J.C. and M.C.; writing—review and editing, J.P.C., J.C., J.J.S. and M.C. All authors have read and agreed to the published version of the manuscript.

Funding: This research was funded by the EU SUDOE, grant number SOE2/P5E0804, project OPEN2PRESERVE.

Data Availability Statement: The data that support the findings of this study are available from the corresponding author, upon reasonable request.

Acknowledgments: The authors acknowledge the Portuguese Foundation for Science and Technology (FCT) for financial support through national funds to CITAB UIDB/04033/2020 (<https://doi.org/10.54499/UIDB/04033/2020>), Innov4Agro LA/P/0126/2020 (<https://doi.org/10.54499/LA/P/0126/2020>), CIMO UIDB/00690/2020 (<https://doi.org/10.54499/UIDB/00690/2020>), and SusTEC LA/P/0007/2020 (<https://doi.org/10.54499/LA/P/0007/2020>). The authors also acknowledge the E-OBS dataset from the EU-FP6 project UERRA (<http://www.uerra.eu> accessed on 24 July 2024) and the Copernicus Climate Change Service and the data providers in the ECA&D project (<https://www.ecad.eu> accessed on 24 July 2024).

Conflicts of Interest: The authors declare no conflicts of interest.

References

1. Tonini, M.; Parente, J.; Pereira, M.G. Global Assessment of Rural–Urban Interface in Portugal Related to Land Cover Changes. *Nat. Hazards Earth Syst. Sci.* **2018**, *18*, 1647–1664. [\[CrossRef\]](#)
2. San-Miguel-Ayanz, J.; Durrant, T.; Boca, R.; Libertà, G.; Branco, A.; De Rigo, D.; Ferrari, D.; Maianti, P.; Artés Vivancos, T.; Oom, D.; et al. *Forest Fires in Europe, Middle East and North Africa 2019*; Publications Office of the European Union: Luxembourg, 2020; ISBN 978-92-76-23209-4.
3. Nikolaj Nielsen Europe’s Wildfire Destruction Set to Hit New Record. Available online: <https://euobserver.com/green-economy/155777> (accessed on 18 October 2022).
4. Barbero, M.; Bonin, G.; Loisel, R.; Quézel, P. Changes and Disturbances of Forest Ecosystems Caused by Human Activities in the Western Part of the Mediterranean Basin. *Vegetatio* **1990**, *87*, 151–173. [\[CrossRef\]](#)
5. Alló, M.; Loureiro, M.L. Assessing Preferences for Wildfire Prevention Policies in Spain. *For. Policy Econ.* **2020**, *115*, 102145. [\[CrossRef\]](#)
6. Tangney, R.; Miller, R.G.; Fontaine, J.B.; Veber, W.P.; Ruthrof, K.X.; Miller, B.P. Vegetation Structure and Fuel Dynamics in Fire-Prone, Mediterranean-Type Banksia Woodlands. *For. Ecol. Manag* **2022**, *505*, 119891. [\[CrossRef\]](#)
7. Fernández-Alonso, J.M.; Vega, J.A.; Jiménez, E.; Ruiz-González, A.D.; Álvarez-González, J.G. Spatially Modeling Wildland Fire Severity in Pine Forests of Galicia, Spain. *Eur. J. For. Res.* **2017**, *136*, 105–121. [\[CrossRef\]](#)
8. Keane, R.E. Describing Wildland Surface Fuel Loading for Fire Management: A Review of Approaches, Methods and Systems. *Int. J. Wildland Fire* **2012**, *22*, 51–62. [\[CrossRef\]](#)
9. Russell, A.; Fontana, N.; Hoecker, T.; Kamanu, A.; Majumder, R.; Stephens, J.; Young, A.M.; Cravens, A.E.; Giardina, C.; Hiers, K.; et al. A Fire-Use Decision Model to Improve the United States’ Wildfire Management and Support Climate Change Adaptation. *Cell Rep. Sustain.* **2024**, *1*, 100125. [\[CrossRef\]](#)
10. Agee, J.K.; Skinner, C.N. Basic Principles of Forest Fuel Reduction Treatments. *For. Ecol. Manag* **2005**, *211*, 83–96. [\[CrossRef\]](#)
11. Castro, M.; Ameray, A.; Castro, J.P. A New Approach to Quantify Grazing Pressure under Mediterranean Pastoral Systems Using GIS and Remote Sensing. *Int. J. Remote Sens.* **2020**, *41*, 5371–5387. [\[CrossRef\]](#)
12. Ameray, A.; Castro, J.P.; Castro, M. Potential Greenhouse Gas Emissions Mitigation through Increased Grazing Pressure: A Case Study in North Portugal. *Carbon Manag* **2022**, *13*, 142–153. [\[CrossRef\]](#)
13. Múgica, L.; Canals, R.M.; San Emeterio, L.; Peralta, J. Decoupling of Traditional Burnings and Grazing Regimes Alters Plant Diversity and Dominant Species Competition in High-Mountain Grasslands. *Sci. Total Environ.* **2021**, *790*, 147917. [\[CrossRef\]](#) [\[PubMed\]](#)
14. Múgica, L.; Canals, R.M.; San Emeterio, L.; Mosquera-Losada, M.R.; Torres, F.; Plaixats, J.; Castro, M.; Robles, A.B.; Sáez, J.L.; Aguerre, C.; et al. Leire Sustainable Management Model for the Preservation of Valuable Open Mountain Areas: The Open2preserve Project. In Proceedings of the 29th General Meeting of the European Grassland Federation, Caen, France, 26–30 June 2022.
15. Velamazán, M.; Perea, R.; Bugalho, M.N. Ungulates and Ecosystem Services in Mediterranean Woody Systems: A Semi-Quantitative Review. *J. Nat. Conserv.* **2020**, *55*, 125837. [\[CrossRef\]](#)

16. Mancilla-Leytón, J.M.; Pino Mejías, R.; Martín Vicente, A. Do Goats Preserve the Forest? Evaluating the Effects of Grazing Goats on Combustible Mediterranean Scrub. *Appl. Veg. Sci.* **2013**, *16*, 63–73. [\[CrossRef\]](#)
17. Mancilla-Leytón, J.M.; Hernando, C.; Cambrollé, J.; Muñoz-Vallés, S.; Pino-Mejías, R.; Vicente, Á.M. Can Shrub Flammability Be Affected by Goat Grazing? Flammability Parameters of Mediterranean Shrub Species under Grazing. *Sustainability* **2021**, *13*, 1555. [\[CrossRef\]](#)
18. Insausti, K.; Beldarrain, L.R.; Lavín, M.P.; Aldai, N.; Mantecón, Á.R.; Sáez, J.L.; Canals, R.M. Horse Meat Production in Northern Spain: Ecosystem Services and Sustainability in High Nature Value Farmland. *Anim. Front.* **2021**, *11*, 47–54. [\[CrossRef\]](#) [\[PubMed\]](#)
19. Fulkerson, W.J.; McKean, K.; Nandra, K.S.; Barchia, I.M.; Fulkerson, W.J.; McKean, K.; Nandra, K.S.; Barchia, I.M. Benefits of Accurately Allocating Feed on a Daily Basis to Dairy Cows Grazing Pasture. *Aust. J. Exp. Agric.* **2005**, *45*, 331–336. [\[CrossRef\]](#)
20. Lentile, L.B.; Holden, Z.A.; Smith, A.M.S.; Falkowski, M.J.; Hudak, A.T.; Morgan, P.; Lewis, S.A.; Gessler, P.E.; Benson, N.C. Remote Sensing Techniques to Assess Active Fire Characteristics and Post-Fire Effects. *Int. J. Wildland Fire* **2006**, *15*, 319–345. [\[CrossRef\]](#)
21. Rudd, J.; Roberson, G.; Classen, J. Application of Satellite, Unmanned Aircraft System, and Ground-Based Sensor Data for Precision Agriculture: A Review. In Proceedings of the 2017 ASABE Annual International Meeting. American Society of Agricultural and Biological Engineers, Spokane, WA, USA, 16–19 July 2017.
22. Saponaro, M.; Tarantino, E. LULC Classification Performance of Supervised and Unsupervised Algorithms on UAV-Orthomosaics. In Proceedings of the Computational Science and Its Applications—ICCSA 2022 Workshops, Malaga, Spain, 4–7 July 2022; Gervasi, O., Murgante, B., Misra, S., Rocha, A.M.A.C., Garau, C., Eds.; Springer International Publishing: Cham, Switzerland, 2022; pp. 311–326.
23. Anderson, K.; Gaston, K.J. Lightweight Unmanned Aerial Vehicles Will Revolutionize Spatial Ecology. *Front. Ecol. Environ.* **2013**, *11*, 138–146. [\[CrossRef\]](#) [\[PubMed\]](#)
24. de Castro, A.I.; Shi, Y.; Maja, J.M.; Peña, J.M. UAVs for Vegetation Monitoring: Overview and Recent Scientific Contributions. *Remote Sens.* **2021**, *13*, 2139. [\[CrossRef\]](#)
25. Poulter, B.; Frank, D.; Ciais, P.; Myneni, R.B.; Andela, N.; Bi, J.; Broquet, G.; Canadell, J.G.; Chevallier, F.; Liu, Y.Y.; et al. Contribution of Semi-Arid Ecosystems to Interannual Variability of the Global Carbon Cycle. *Nature* **2014**, *509*, 600–603. [\[CrossRef\]](#)
26. Mao, P.; Qin, L.; Hao, M.; Zhao, W.; Luo, J.; Qiu, X.; Xu, L.; Xiong, Y.; Ran, Y.; Yan, C.; et al. An Improved Approach to Estimate Above-Ground Volume and Biomass of Desert Shrub Communities Based on UAV RGB Images. *Ecol. Indic.* **2021**, *125*, 107494. [\[CrossRef\]](#)
27. Zhao, Y.; Liu, X.; Wang, Y.; Zheng, Z.; Zheng, S.; Zhao, D.; Bai, Y. UAV-Based Individual Shrub Aboveground Biomass Estimation Calibrated against Terrestrial LiDAR in a Shrub-Encroached Grassland. *Int. J. Appl. Earth Obs. Geoinf.* **2021**, *101*, 102358. [\[CrossRef\]](#)
28. Abdullah, M.M.; Al-Ali, Z.M.; Abdullah, M.T.; Srinivasan, S.; Assi, A.T.; Al Atiqi, S. Investigating the Applicability of UAVs in Characterizing Desert Shrub Biomass and Developing Biological Indicators for the Selection of Suitable Revegetation Sites. *J. Environ. Manag.* **2021**, *288*, 112416. [\[CrossRef\]](#) [\[PubMed\]](#)
29. Villoslada Pecina, M.; Bergamo, T.F.; Ward, R.D.; Joyce, C.B.; Sepp, K. A Novel UAV-Based Approach for Biomass Prediction and Grassland Structure Assessment in Coastal Meadows. *Ecol. Indic.* **2021**, *122*, 107227. [\[CrossRef\]](#)
30. Zhang, H.; Sun, Y.; Chang, L.; Qin, Y.; Chen, J.; Qin, Y.; Du, J.; Yi, S.; Wang, Y. Estimation of Grassland Canopy Height and Aboveground Biomass at the Quadrat Scale Using Unmanned Aerial Vehicle. *Remote Sens.* **2018**, *10*, 851. [\[CrossRef\]](#)
31. Théau, J.; Lauzier-Hudon, É.; Aubé, L.; Devillers, N. Estimation of Forage Biomass and Vegetation Cover in Grasslands Using UAV Imagery. *PLoS ONE* **2021**, *16*, e0245784. [\[CrossRef\]](#) [\[PubMed\]](#)
32. Da Pereira, F.R.S.; de Lima, J.P.; Freitas, R.G.; Dos Reis, A.A.; Do Amaral, L.R.; Figueiredo, G.K.D.A.; Lamparelli, R.A.C.; Magalhães, P.S.G. Nitrogen Variability Assessment of Pasture Fields under an Integrated Crop-Livestock System Using UAV, PlanetScope, and Sentinel-2 Data. *Comput. Electron. Agric.* **2022**, *193*, 106645. [\[CrossRef\]](#)
33. Lussem, U.; Bolten, A.; Menne, J.; Gnyp, M.L.; Schellberg, J.; Bareth, G. Estimating Biomass in Temperate Grassland with High Resolution Canopy Surface Models from UAV-Based RGB Images and Vegetation Indices. *JARS* **2019**, *13*, 034525. [\[CrossRef\]](#)
34. Possoch, M.; Bieker, S.; Hoffmeister, D.; Bolten, A.; Schellberg, J.; Bareth, G. Multi-Temporal Crop Surface Models Combined with the RGB Vegetation Index from Uav-Based Images for Forage Monitoring in Grassland. *ISPRS—Int. Arch. Photogramm. Remote Sens. Spat. Inf. Sci.* **2016**, *41B1*, 991–998. [\[CrossRef\]](#)
35. Zhang, H.; Tang, Z.; Wang, B.; Meng, B.; Qin, Y.; Sun, Y.; Lv, Y.; Zhang, J.; Yi, S. A Non-Destructive Method for Rapid Acquisition of Grassland Aboveground Biomass for Satellite Ground Verification Using UAV RGB Images. *Glob. Ecol. Conserv.* **2022**, *33*, e01999. [\[CrossRef\]](#)
36. Wijesingha, J.; Astor, T.; Schulze-Brüninghoff, D.; Wengert, M.; Wachendorf, M. Predicting Forage Quality of Grasslands Using UAV-Borne Imaging Spectroscopy. *Remote Sens.* **2020**, *12*, 126. [\[CrossRef\]](#)
37. Capolupo, A.; Kooistra, L.; Berendonk, C.; Boccia, L.; Suomalainen, J. Estimating Plant Traits of Grasslands from UAV-Acquired Hyperspectral Images: A Comparison of Statistical Approaches. *ISPRS Int. J. Geo-Inf.* **2015**, *4*, 2792–2820. [\[CrossRef\]](#)
38. Insua, J.R.; Utsumi, S.A.; Basso, B. Estimation of Spatial and Temporal Variability of Pasture Growth and Digestibility in Grazing Rotations Coupling Unmanned Aerial Vehicle (UAV) with Crop Simulation Models. *PLoS ONE* **2019**, *14*, e0212773. [\[CrossRef\]](#) [\[PubMed\]](#)

39. Polley, H.W.; Kolodziejczyk, C.A.; Jones, K.A.; Derner, J.D.; Augustine, D.J.; Smith, D.R. UAV—Enabled Quantification of Grazing-Induced Changes in Uniformity of Green Cover on Semiarid and Mesic Grasslands. *Rangel. Ecol. Manag.* **2022**, *80*, 68–77. [\[CrossRef\]](#)
40. Alvarez-Hess, P.S.; Thomson, A.L.; Karunaratne, S.B.; Douglas, M.L.; Wright, M.M.; Heard, J.W.; Jacobs, J.L.; Morse-McNabb, E.M.; Wales, W.J.; Auld, M.J. Using Multispectral Data from an Unmanned Aerial System to Estimate Pasture Depletion during Grazing. *Anim. Feed. Sci. Technol.* **2021**, *275*, 114880. [\[CrossRef\]](#)
41. Batistoti, J.; Marcato Junior, J.; Ítavo, L.; Matsubara, E.; Gomes, E.; Oliveira, B.; Souza, M.; Siqueira, H.; Salgado Filho, G.; Akiyama, T.; et al. Estimating Pasture Biomass and Canopy Height in Brazilian Savanna Using UAV Photogrammetry. *Remote Sens.* **2019**, *11*, 2447. [\[CrossRef\]](#)
42. Surový, P.; Ribeiro, N.A.; Panagiotidis, D. Estimation of Positions and Heights from UAV-Sensed Imagery in Tree Plantations in Agrosilvopastoral Systems. *Int. J. Remote Sens.* **2018**, *39*, 4786–4800. [\[CrossRef\]](#)
43. Carvajal-Ramírez, F.; Marques da Silva, J.R.; Agüera-Vega, F.; Martínez-Carricondo, P.; Serrano, J.; Moral, F.J. Evaluation of Fire Severity Indices Based on Pre- and Post-Fire Multispectral Imagery Sensed from UAV. *Remote Sens.* **2019**, *11*, 993. [\[CrossRef\]](#)
44. Mayr, M.J.; Malß, S.; Ofner, E.; Samimi, C. Disturbance Feedbacks on the Height of Woody Vegetation in a Savannah: A Multi-Plot Assessment Using an Unmanned Aerial Vehicle (UAV). *Int. J. Remote Sens.* **2018**, *39*, 4761–4785. [\[CrossRef\]](#)
45. Olsoy, P.J.; Glenn, N.F.; Clark, P.E.; Derryberry, D.R. Aboveground Total and Green Biomass of Dryland Shrub Derived from Terrestrial Laser Scanning. *ISPRS J. Photogramm. Remote Sens.* **2014**, *88*, 166–173. [\[CrossRef\]](#)
46. Greaves, H.E.; Vierling, L.A.; Eitel, J.U.H.; Boelman, N.T.; Magney, T.S.; Prager, C.M.; Griffin, K.L. High-Resolution Mapping of Aboveground Shrub Biomass in Arctic Tundra Using Airborne Lidar and Imagery. *Remote Sens. Environ.* **2016**, *184*, 361–373. [\[CrossRef\]](#)
47. Passalacqua, N.G.; Aiello, S.; Bernardo, L.; Gargano, D. Monitoring Biomass in Two Heterogeneous Mountain Pasture Communities by Image Based 3D Point Cloud Derived Predictors. *Ecol. Indic.* **2021**, *121*, 107126. [\[CrossRef\]](#)
48. Maesano, M.; Santopuoli, G.; Moresi, F.V.; Matteucci, G.; Lasserre, B.; Scarascia Mugnozza, G. Above Ground Biomass Estimation from UAV High Resolution RGB Images and LiDAR Data in a Pine Forest in Southern Italy. *Iforest—Biogeosci. For.* **2022**, *15*, 451. [\[CrossRef\]](#)
49. Matese, A.; Toscano, P.; Di Gennaro, S.F.; Genesio, L.; Vaccari, F.P.; Primicerio, J.; Belli, C.; Zaldei, A.; Bianconi, R.; Gioli, B. Intercomparison of UAV, Aircraft and Satellite Remote Sensing Platforms for Precision Viticulture. *Remote Sens.* **2015**, *7*, 2971–2990. [\[CrossRef\]](#)
50. McClelland, M.P.; van Aardt, J.; Hale, D. Manned Aircraft versus Small Unmanned Aerial System—Forestry Remote Sensing Comparison Utilizing Lidar and Structure-from-Motion for Forest Carbon Modeling and Disturbance Detection. *JARS* **2019**, *14*, 022202. [\[CrossRef\]](#)
51. Canfield, R.H. Application of the Line Interception Method in Sampling Range Vegetation. *J. For.* **1941**, *39*, 388–394. [\[CrossRef\]](#)
52. Breckenridge, R.P.; Dakins, M.E. Evaluation of Bare Ground on Rangelands Using Unmanned Aerial Vehicles: A Case Study. *GISci. Remote Sens.* **2011**, *48*, 74–85. [\[CrossRef\]](#)
53. Figueiredo, T. *De Uma Panorâmica Sobre os Recursos Pedológicos do Nordeste Transmontano*; Instituto Politécnico de Bragança, Escola Superior Agrária: Coimbra, Portugal, 2013; ISBN 978-972-745-138-8.
54. FAO; FAO/UNESCO. *Soil Map of the World. Revised Legend, with Corrections and Updates*; World Soil Resources Report; FAO: Rome, Italy, 1988; Volume 60, ISBN 90-6672-057-3.
55. Cornes, R.C.; van der Schrier, G.; van den Besselaar, E.J.M.; Jones, P.D. An Ensemble Version of the E-OBS Temperature and Precipitation Data Sets. *J. Geophys. Res. Atmos.* **2018**, *123*, 9391–9409. [\[CrossRef\]](#)
56. Castro, M.; Castro, J.P.; Castro, J. Understory Clearing in Open Grazed Mediterranean Oak Forests: Assessing the Impact on Vegetation. *Sustainability* **2022**, *14*, 10979. [\[CrossRef\]](#)
57. Rouse, J.W., Jr.; Haas, R.H.; Schell, J.A.; Deering, D.W. Monitoring Vegetation Systems in The Great Plains with ERTS. In Proceedings of the Goddard Space Flight Center 3rd ERTS-1 Symp., Washington, DC, USA, 10–14 December 1974; NASA: Washington, DC, USA, 1974; Volume 1, pp. 309–317.
58. Hengl, T. Finding the Right Pixel Size. *Comput. Geosci.* **2006**, *32*, 1283–1298. [\[CrossRef\]](#)
59. Pádua, L.; Marques, P.; Adão, T.; Hruška, J.; Peres, E.; Morais, R.; Sousa, A.; Sousa, J.J. UAS-Based Imagery and Photogrammetric Processing for Tree Height and Crown Diameter Extraction. In Proceedings of the International Conference on Geoinformatics and Data Analysis, Prague, Czech Republic, 20–22 April 2018; ACM: New York, NY, USA, 2018; pp. 87–91.
60. Matese, A.; Di Gennaro, S.F.; Berton, A. Assessment of a Canopy Height Model (CHM) in a Vineyard Using UAV-Based Multispectral Imaging. *Int. J. Remote Sens.* **2016**, *38*, 2150–2160. [\[CrossRef\]](#)
61. Marques, P.; Pádua, L.; Adão, T.; Hruška, J.; Sousa, J.J.; Peres, E.; Martins, L.M.; Sousa, A. *Automatic Chestnut Trees Monitoring by Aerial Photographs Obtained by Unmanned Aerial Vehicle*; UTAD: Vila Real, Portugal, 2017; pp. 32–33.
62. Pádua, L.; Adão, T.; Guimarães, N.; Sousa, A.; Peres, E.; Sousa, J.J. Post-Fire Forestry Recovery Monitoring Using High-Resolution Multispectral Imagery From Unmanned Aerial Vehicles. In Proceedings of the ISPRS—International Archives of the Photogrammetry, Remote Sensing and Spatial Information Sciences, Prague, Czech Republic, 3–6 September 2019; Copernicus GmbH: Göttingen, Germany, 2019; Volume XLII-3-W8, pp. 301–305.
63. Pádua, L.; Guimarães, N.; Adão, T.; Sousa, A.; Peres, E.; Sousa, J.J. Effectiveness of Sentinel-2 in Multi-Temporal Post-Fire Monitoring When Compared with UAV Imagery. *ISPRS Int. J. Geo-Inf.* **2020**, *9*, 225. [\[CrossRef\]](#)

64. Gitelson, A.A.; Kaufman, Y.J.; Merzlyak, M.N. Use of a Green Channel in Remote Sensing of Global Vegetation from EOS-MODIS. *Remote Sens. Environ.* **1996**, *58*, 289–298. [\[CrossRef\]](#)
65. McIntosh, M.M.; Cibils, A.F.; Estell, R.E.; Gong, Q.; Cao, H.; Gonzalez, A.L.; Nyamuryekung'e, S.; Spiegel, S.A. Can Cattle Geolocation Data Yield Behavior-Based Criteria to Inform Precision Grazing Systems on Rangeland? *Livest. Sci.* **2022**, *255*, 104801. [\[CrossRef\]](#)
66. Abdulai, G.; Sama, M.; Jackson, J. A Preliminary Study of the Physiological and Behavioral Response of Beef Cattle to Unmanned Aerial Vehicles (UAVs). *Appl. Anim. Behav. Sci.* **2021**, *241*, 105355. [\[CrossRef\]](#)
67. Sun, Y.; Yi, S.; Hou, F.; Luo, D.; Hu, J.; Zhou, Z. Quantifying the Dynamics of Livestock Distribution by Unmanned Aerial Vehicles (UAVs): A Case Study of Yak Grazing at the Household Scale. *Rangel. Ecol. Manag* **2020**, *73*, 642–648. [\[CrossRef\]](#)
68. Barbedo, J.G.A.; Koenigkan, L.V.; Santos, T.T.; Santos, P.M. A Study on the Detection of Cattle in UAV Images Using Deep Learning. *Sensors* **2019**, *19*, 5436. [\[CrossRef\]](#) [\[PubMed\]](#)
69. Shao, W.; Kawakami, R.; Yoshihashi, R.; You, S.; Kawase, H.; Naemura, T. Cattle Detection and Counting in UAV Images Based on Convolutional Neural Networks. *Int. J. Remote Sens.* **2020**, *41*, 31–52. [\[CrossRef\]](#)
70. Adar, S.; Sternberg, M.; Paz-Kagan, T.; Henkin, Z.; Dovrat, G.; Zaady, E.; Argaman, E. Estimation of Aboveground Biomass Production Using an Unmanned Aerial Vehicle (UAV) and VEN μ S Satellite Imagery in Mediterranean and Semiarid Rangelands. *Remote Sens. Appl. Soc. Environ.* **2022**, *26*, 100753. [\[CrossRef\]](#)
71. Polley, H.W.; Kolodziejczyk, C.A.; Jones, K.A.; Smith, D.R. Grazing Treatment Influences Recovery of Mesic Grassland from Seasonal Drought: An Assessment Using Unmanned Aerial Vehicle—Enabled Remote Sensing. *Rangel. Ecol. Manag* **2022**, *82*, 12–19. [\[CrossRef\]](#)
72. Pádua, L.; Guimarães, N.; Adão, T.; Marques, P.; Peres, E.; Sousa, A.; Sousa, J.J. Classification of an Agrosilvopastoral System Using RGB Imagery from an Unmanned Aerial Vehicle. In Proceedings of the Progress in Artificial Intelligence, Vila Real, Portugal, 3–6 September 2019; Moura Oliveira, P., Novais, P., Reis, L.P., Eds.; Springer International Publishing: Cham, Switzerland, 2019; pp. 248–257.
73. Lu, B.; He, Y. Species Classification Using Unmanned Aerial Vehicle (UAV)-Acquired High Spatial Resolution Imagery in a Heterogeneous Grassland. *ISPRS J. Photogramm. Remote Sens.* **2017**, *128*, 73–85. [\[CrossRef\]](#)
74. Trenčanová, B.; Proença, V.; Bernardino, A. Development of Semantic Maps of Vegetation Cover from UAV Images to Support Planning and Management in Fine-Grained Fire-Prone Landscapes. *Remote Sens.* **2022**, *14*, 1262. [\[CrossRef\]](#)

Disclaimer/Publisher's Note: The statements, opinions and data contained in all publications are solely those of the individual author(s) and contributor(s) and not of MDPI and/or the editor(s). MDPI and/or the editor(s) disclaim responsibility for any injury to people or property resulting from any ideas, methods, instructions or products referred to in the content.